NUMERICAL CALCULATION OF THE UNSTEADY TWO-DIMENSIONAL INCOMPRESSIBLE FLOW AROUND NACA AIRFOILS USING THE VORTEX METHOD

Daniel Fonseca de Carvalho e Silva
e-mail: danfcs@yahoo.com

Gustavo César Rachid Bodstein
e-mail: gustavo@serv.com.ufrj.br

Department of Mechanical Engineering – Poli/COPPE
Federal University of Rio de Janeiro
Centro de Tecnologia, Bloco G, sala 204 – Ilha do Fundão
21945-970 Rio de Janeiro, RJ – Brazil

Abstract. *Unsteady, incompressible, high Reynolds-number flows around a two-dimensional airfoil set at an angle of attack are characterized by an attached boundary layer on the airfoil surface and a linear behavior of the lift coefficent with the angle of atack, when the angle of attack is small. For large angles of attack, massive boundary layer separation occurs together with a decrease in the lift coefficient and the formation of an oscillatory airfoil wake. In this paper, a mesh-free Discrete Vortex Method is used to simulate the unsteady, two-dimensional, incompressible and high Reynolds number flow around a NACA 0012 airfoil in the small angle of attack regime. The flow vorticity is modeled as a cloud of Lamb vortices, whereas the airfoil contribution to the flow is calculated using a piecewise-continuous linear-vortex panel method. The dynamics of the entire vortex cloud is computed using the convection-diffusion splitting algorithm for the vorticity equation, where the diffusion transport is simulated using the random walk method and the convection transport is calculated using the the Biot-Savart law and a lagrangian time-marching scheme. Results for the aerodynamic loads acting on the airfoil for several values of the angle of attack are shown in comparison with other results available in the literature.*

Keywords: *Vortex Method, Panel Method, Airfoil, Unsteady Wake, Aerodynamics*

1. Introduction

The simulation of unsteady, incompressible, high Reynolds-number flows around a two-dimensional airfoil set at an angle of attack finds numerous applications in aeronautical and mechanical engineering. For these flows, aerodynamic properties, such as the maximum lift coefficient, the separation point and the oscillatory behavior of the wake cannot be predicted by classical potential flow theory for a wide range of angles of attack. When the angle of attack is large, the boundary layer separates from the airfoil surface, remaining attached to the surface only when the angle of attack is small. Due to the physical complexity, numerical methods appear as a natural approach to handle flows of this type.

Complex fluid flow calculations around bodies remain a challenge for modern Computational Fluid Dynamics (CFD) models and they are still the object of theoretical research. The most popular commercial codes use eulerian numerical methods, such as finite difference, finite volume or finite element methods, for the numerical solution of the Navier-Stokes equations. This paper presents results of several simulations of unsteady, incompressible, high Reynolds-number flows around a two-dimensional NACA 0012 airfoil, in the small angle of attack range, using a lagrangian mesh-free discrete vortex method. This airfoil has been chosen because of its numerous applications to aeronautical and turbomachinery engineering. The first viscous algorithm of the lagrangian mesh-free discrete vortex method has been originally developed by Chorin (1973). Sarpkaya (1994) presents an excellent review of the historical developments of the vortex method, the most important models that are still in use nowadays, and most of the articles that have been published on vortex methods and its applications. Recent developments of the vortex method in the Brazilian scenario have been carried out by Guedes (2003), Mustto (2004) and Alcântara Pereira (1999, 2002), to cite just a few. Akbari and Price (2003) apply the vortex method in association with conformal transformation to simulate the flow around the NACA0012 airfoil.

2. The Discrete Vortex Method

The vortex method is based on the discretization of the vorticity field into discrete vortex blobs and calculating their positions for each time step based on the velocity-vorticity relations. The most important advantage of this method is that a grid is not necessary, and the simulation takes place only in the regions where the vorticity has strong influence on the flow, *i.e.,* the boundary layer and the wake downstream the body.

The governing equations for an incompressible flow with constant properties, in the non-dimensional form, considering that the influence of body forces is negligible, can be written as:

$$\nabla \cdot \mathbf{q} = 0\,, \qquad \text{[Continuity equation]}, \tag{1}$$

$$\frac{\partial \mathbf{q}}{\partial t} + \mathbf{q} \cdot \nabla \mathbf{q} = -\frac{1}{2}\nabla p + \frac{1}{Re}\nabla^2 \mathbf{q}\,, \quad \text{[Navier-Stokes equation]}, \tag{2}$$

where $Re = \dfrac{Qc}{\nu}$.

In these equations, **q** is the velocity vector field, p is the absolute pressure, Re is the Reynolds number based on c, the airfoil chord length, ν is the fluid kinematic viscosity. This equations are subjected to the following boundary conditions: **q** = **0** on the body surface – this condition represents the zero normal flow and the no-slip condition for a body at rest; and **q** = $\mathbf{Q}_\infty$ at infinity, where $\mathbf{Q}_\infty$ is the undisturbed incident velocity field. Additionally, the initial condition is **q** = $\mathbf{Q}_\infty$ at t = 0^+. Figure 1 illustrates this physical situation.

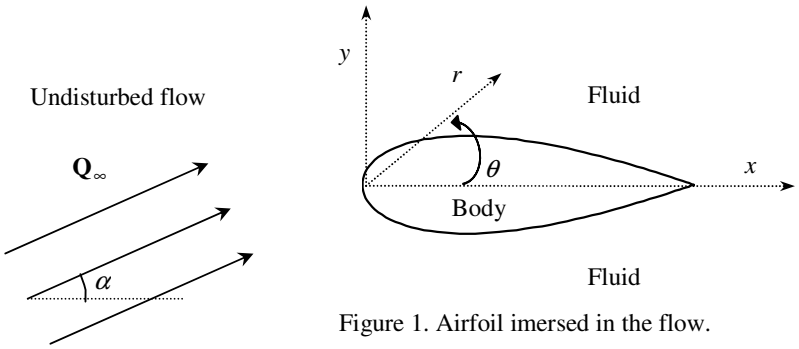

Figure 1. Airfoil imersed in the flow.

Taking the curl of Eq.(2) eliminates de pressure terms and results in the Vorticity Transport Equation, that is,

$$\frac{\partial \boldsymbol{\omega}}{\partial t} + \mathbf{q} \cdot \nabla \boldsymbol{\omega} = \boldsymbol{\omega}.\nabla \mathbf{q} + \frac{1}{Re}\nabla^2 \boldsymbol{\omega}\,. \tag{3}$$

For two-dimensional flows the vorticity vector, $\boldsymbol{\omega} = \nabla \times \mathbf{q}$, becomes a scalar, with only one non-zero component normal to the plane of the flow. The first term on the right-hand side of the Eq. (3) also becomes zero. Rewriting this equation, we obtain

$$\frac{\partial \omega}{\partial t} + \mathbf{q} \cdot \nabla \omega = \frac{1}{Re}\nabla^2 \omega\,. \tag{4}$$

This equation represents the vorticity transport that occurs in the flow subject to convective and diffusive effects. Although both effects take place at the same time in a real flow, it is convenient, for numerical reasons, to use the convection-diffusion splitting algorithm proposed by Chorin (1973), where Eq. (4) is first solved ignoring the diffusive effects and then Eq. (4) is solved ignoring convective effects, during the same time interval Δt. This way, it is possible to obtain an approximate vorticity field for each time step. This approximation is good as long Δt is small. The split convective-diffusive equations are written below, followed by a simplified schematic diagram of the numerical method shown in Fig. 2.

$$\frac{\partial \omega}{\partial t} + \mathbf{q} \cdot \nabla \omega = 0 \qquad \text{[Convection]} \tag{5a}$$

$$\frac{\partial \omega}{\partial t} = \frac{1}{Re}\nabla^2 \omega \qquad \text{[Diffusion]} \tag{5b}$$

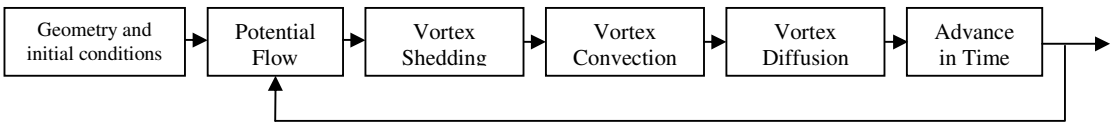

Figure 2. Simplified schematic diagram of the algorithm.

3. Potential Flow – The Panel Method

For the potential flow, the velocity field can be written as the gradient of a scalar velocity potential, $\mathbf{q} = \nabla\phi$. The velocity potential ϕ is a solution of Laplace´s equation, obtained from the substitution of the equation above into the continuity equation for incompressible flow, Eq. (1). Thus we can write

$$\nabla^2\phi = 0 \quad \text{in the fluid region.} \tag{6}$$

Equation (6) is subject to the zero normal flow boundary conditions, $\nabla\phi \cdot \mathbf{n} = 0$ on the airfoil surface, and the boundary condition at infinity, $\nabla\phi = \mathbf{Q}_\infty$. This boundary value problem is solved using the panel method, originally devised by Martensen (1931), and described in details in Katz and Plotkin (2001). The Panel method has the advantage that it may be applied to complex geometries. The airfoil geometry is divided into plane segments, called panels, each one with length Δl_i. The point in the middle of the panel is the control point, where the boundary condition must be satisfied, and the endpoints are the panel nodes. Among the possible choices for the solution of Laplace's equation, we choose the vortex singularity with linear distribution of vorticity along the panel length. The linear vortex strength is calculated so that the zero flow normal boundary condition is satisfied at all the panel control points. This formulation yields a linear system of N algebraic equations, one for each control point, and $N + 1$ unknowns, the panel vorticity strength at the panel nodes. This system needs an extra equation to be solved uniqueley, which is the Kutta condition, for steady potential flows, or the conservation of circulation condition, for unsteady flows such as the ones studied here. The linear vortex distribution is employed in this work based on the studies published by Pereira *et al*. (2004) and Pereira and Bodstein (2004). The airfoil discretization is made so that the leading and trailing edge regions have a fine concentration of panels, as recommended by Lewis (1991) and Katz and Plotkin (2001). In these regions, the flow experiences high velocity and pressure gradients.

4. Vortex Shedding

The vorticity generation process in the solid-fluid interface is modeled using the solution obtained in section 3 above for vorticity distribution on the panels. Once the vorticity distribution on the panels is determined, discrete vortex blobs are generated near the solid surface, with strength equal to the mean vorticity on the panel $[(\gamma_i + \gamma_{i+1})/2]\Delta l_i$ and positioned at a small distance ε perpendicular to each panel control point, as shown in Fig. 3. These vortices are free to be convected and diffused by the flow, simulating the vorticity shedding into the wake. The value of ε is given by the Lamb vortex core (Mustto, 2004), that is,

$$\varepsilon = \sigma_0 = 4{,}48364\sqrt{\frac{\Delta t}{Re}}\,. \tag{7}$$

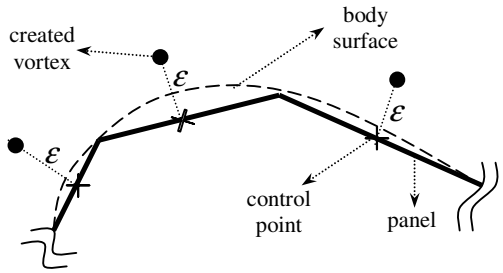

Figure 3. Vorticity shedding on the body surface.

5. Vorticity Convection – The Biot-Savart Law

The calculation of the convective velocity field is carried out by the velocities induced by each vortex blob, using the Lamb vortex model to avoid the singular velocities at the core of Point vortices. The velocities induced by a vortex j at a point (x_i, z_i) of the fluid domain are calculated as

$$u_{ij} = \begin{cases} \Gamma_j U_{ij} & \text{if} \quad r_{ij} \geq \sigma_0 \\ \Gamma_j U_{ij}\left[1 - \exp\left(-\lambda(r_{ij}/\sigma_0)^2\right)\right] & \text{if} \quad r_{ij} < \sigma_0 \end{cases}, \tag{8a}$$

$$v_{ij} = \begin{cases} \Gamma_j V_{ij} & \text{if} \quad r_{ij} \geq \sigma_0 \\ \Gamma_j V_{ij} \left[1 - \exp\left(-\lambda (r_{ij}/\sigma_0)^2 \right) \right] & \text{if} \quad r_{ij} < \sigma_0 \end{cases}, \tag{8b}$$

where $U_{ij} = \frac{1}{2\pi} \frac{z_i - z_j}{r_{ij}^{\,2}}$, $V_{ij} = -\frac{1}{2\pi} \frac{x_i - x_j}{r_{ij}^{\,2}}$, $r_{ij} = \sqrt{(x_i - x_j)^2 + (z_i - z_j)^2}$ and $\lambda = 5{,}02572$.

In Eqs. (8a,b), Γ_j is the vortex strength and σ_0 is the vortex core radius, given by Eq. (7). The total induced velocity must be calculated adding three different contributions: the first from the vortex cloud; the second from the panels, which represent the body influence on the flow; and the last one from the undisturbed constant velocity field $\mathbf{Q}_\infty$.

6. Vorticity Diffusion –The Random Walk Method

Equation (5b) has an analytical solution for the vorticity field of a point vortex that is initially irrotational and whose vorticity spreads out purely by the action of viscosity. This solution is given by

$$\omega(r,t) = Re \frac{\Gamma}{4\pi t} \exp\left[-Re \frac{r^2}{4t} \right]; \text{ where } r = \sqrt{x^2 + y^2}\ . \tag{9}$$

Considering that the vortex cloud is represented by a large number of discrete vortices, this equation can be interpreted as the probability to find a vortex at a given spatial region at a given time (Lewis, 1991). Under this assumption, the diffusive radial and circumferential displacements of the discrete vortex, for high Reynolds numbers flows, can be calculated as

$$\Delta r = \sqrt{\frac{4\Delta t}{Re} \ln\left(\frac{1}{P} \right)} \quad \text{and} \quad \Delta\theta = 2\pi Q\ , \tag{10a,b}$$

where P e Q are randomly generated numbers between 0 and 1 drawn from a uniform probability distribution. In cartesian coordinates, the displacements of each vortex in the x and y directions can be expressed, using Eqs. (10a,b), as

$$\Delta x_D = \Delta r \cos(\Delta\theta) \text{ and } \Delta y_D = \Delta r\, \text{sen}(\Delta\theta)\ . \tag{11a,b}$$

7. Aerodynamic Loads

Calculated on the body surface, Eq. (2) can be written in a direction tangential to body surface s as

$$\frac{\partial q_s}{\partial t} = -\frac{1}{2} \frac{\partial p}{\partial s}\ . \tag{12}$$

Based on the potential flow analysis, the tangential velocity for each surface control point is given by $q_s = -\gamma$. This equation may be substituted into the discretized form of Eq. (12) to furnish

$$\Delta p_i = \frac{2\gamma_i \Delta l_i}{\Delta t}\ . \tag{13}$$

Equation (13) determines the differential pressure at each panel control point. Integrating this equation along the body surface yields

$$p_i = p_0 + \sum_{n=1}^{i} \Delta p_n\ . \tag{14}$$

Choosing the reference pressure p_0 to be $p_0 = 0$ allows for the calculation of each p_i to be carried out at the control points, and the maximum pressure on the body p_s, the stagnation pressure, can be determined. Thus, adding the quantity $(1 - p_s)$ to the pre-calculated values of p_i, the non-dimensional pressure on the body is obtained (Lewis, 1991). The non-dimensional pressure is equivalent to the pressure coefficient, given by

$$C_p = p = \frac{p^*}{\frac{1}{2}\rho Q_\infty^2}, \tag{15}$$

where p^* is the dimensional pressure. Integrating C_p over the body surface and projecting the loads on the parallel and perpendicular flow directions it is possible to calculate the drag and lift coefficients, respectively, according to

$$C_l = \sum_{i=1}^{N} C_{pi}\Delta l_i \,\mathrm{sen}(\alpha+\beta_i) \quad \text{and} \quad C_d = \sum_{i=1}^{N} C_{pi}\Delta l_i \cos(\alpha+\beta_i), \tag{16a,b}$$

where β_i is the inclination and Δl_i is the length of the i-th panel.

8. Time Marching Scheme

For the time marching scheme, it is necessary to use the calculated convective velocity field and the diffusive displacements to evaluate the new position of each vortex in the cloud. Since the random-walk method already provides the diffusive displacement, we only need to integrate the convective velocity field. In this paper we use a first-order Euler scheme and a second-order Adams-Bashforth scheme, given, respectively, by

$$\Delta x_C = u(t)\Delta t \ \text{ and } \ \Delta y_C = v(t)\Delta t, \tag{17a,b}$$

$$\Delta x_C = \left[1{,}5u(t) + 0{,}5u(t-\Delta t)\right]\Delta t \ \text{ and } \ \Delta y_C = \left[1{,}5v(t) + 0{,}5v(t-\Delta t)\right]\Delta t. \tag{18a,b}$$

High order schemes are avoided because of the large additional computational effort imposed on the computation. The Adams-Bashforth scheme requires the use of the velocity field calculated at the previous time step. Therefore, the first step for each nascent vortex is always calculated by the Euler scheme. As soon as the convective displacement is calculated, the new vortex cloud position is evaluated by:

$$x(t+\Delta t) = x(t) + \Delta x_D + \Delta x_C \ \text{ and } \ y(t+\Delta t) = y(t) + \Delta y_D + \Delta y_C. \tag{19a,b}$$

Ocasionally, because of the random walk displacement or the strong curvature of specific body regions, some of the discrete vortices may penetrate into the body. The literature presents two possible solutions for these vortices: the first one is to eliminate them from the flow; the second one is to reflect the vortices back into the flow. The second alternative is applied to the simulations of this paper. This option retains a larger wake resolution and causes better quality of the results.

9. Numerical Considerations

For the solution of the linear system of algebraic equations, an extra equation must be added in order to render the system determined and the solution unique. As pointed out in section 3, we include an equation for the conservation of circulation that expresses Kelvin's theorem. This equation may be written as

$$\sum_{j=1}^{N} \frac{\gamma_j + \gamma_{j+1}}{2}\Delta\ell_j + \sum_{k=1}^{M} \Gamma_k = 0, \tag{20}$$

where N is the number of panels and M is the number of discrete vortices in the vortex cloud, each one with vortex strength Γ_k. Since the fluid flow begins from rest, there are no vortices in the wake at the first time step. Hence, Eq. (20) reduces to

$$\sum_{j=1}^{N} \frac{\gamma_j + \gamma_{j+1}}{2}\Delta\ell_j = 0. \tag{21}$$

For the following time step, the linear vorticity distribution along the body panels is transformed into Lamb vortices, each with strength $\Gamma_k = [(\gamma_i + \gamma_{i+1})/2]\Delta l_i$ and whose sum over all the N vortices is equal to zero. Therefore, the second term in Eq. (20) is zero, and Eq. (20) again reduces to Eq. (21). The same procedure is repeated the following time steps. Thus, Eq. (21) is the one that is used to complete the linear system of algebraic equations. The solution is found using a LU decompositon algorithm.

Another special consideration that must be made concerns the velocities from vortices too close to the body induced at the control points, and vice-versa, velocities from body panels induced at vortices that are too close to the control panel. In both cases, these induced velocities may be unrealistically high, requiring special treatment. Following Lewis (1991), we adopt the following procedure based on the distance from the vortex to the nearest control point r_{jk},. For a panel of length Δl_k, if $r_{jk} < 0.4\ \Delta l_k$, that is, if the vortex is extremely close to the control panel, we use the velocity induced by its image inside the body, located the same distance apart from the panel in the normal direction, to compute the velocity induced at the vortex. If vortex is a little farther from the control point, in the range $0.4\ \Delta l_k \leq r_{jk} < 2.0\ \Delta l_k$, the panel is divided into 5 subpanels, and the induced velocities at the vortex are computed as the sum of the contributions of all subpanels, whereas the velocity at the control point is the average of the velocity induced by the vortex at the control points of each subpanel. If the vortex is even farther, that is, $r_{jk} > 2.0\ \Delta l_k$, the velocity field is calculated using the equations described in the sections above. This simple model has added important improvements to the accuracy of the complete algorithm employed in this work.

10. Results

A computer program has been written to implement the model described above for the simulation of unsteady, two-dimensional, incompressible flows around airfoils. All simulations have been caried out for laminar flows around the NACA 0012 airfoil, in the pre-stall regime, with a Reynolds number of 1.7×10^5.

The numerical parameters used in all cases are: 300 panels; 5 subpanels; the Adams-Bashforth scheme with $\Delta t = 0.025$; and vortex core radius equal to 0.005, calculated from Eq. (7). Figure 4a shows the position of the vortices at the last step of the simulation for a 6-degree angle of attack. From this figure its possible to notice that the flow is attached to the airfoil, as expected for this small angle of attack, and the wake is characterized by the formation of pairs of counter-rotating vortex-like structures. Figure 4b shows the time history of the lift coefficient during the entire simulation. As soon as the numerical transient is over (approximately $t = 3.5$), the lift coefficient starts to oscilate about an average value of 0.42.

As the angle of attack of the incident flow is increased up to 10 degrees, the wake becomes more oscilatory, with large eddies being shed from the airfoil surface, as one can infer from the position of the vortices in the wake at the last step of the computation, shown in Fig. 5a. The wake pattern indicates the onset of boundary layer separation and the development of a bluff-body type behavior of the wake. Figure 5b presents the time variation of the lift coeffcient for this case, indicating a stronger noise-like signal during the initial numerical transient of the simulation than the previous case. After this initial stage, a periodic behavior of the lift coefficient is established around a mean value of about 0.75. In this case, the amplitude of the oscillation of the lift coefficient is higher than in the 6-degree angle-of-attack case. For both cases, the average values of the lift coefficient are computed from $t = 5$, in order to allow the oscillating behavior of the wake to settle in, up to $t = 10$, the last step of the simulation.

Several values of the angle of attack have been simulated, all in the pre-stall range of the angle of attack. The numerical results obtained and a comparison with experiments are shown in Fig. 6. Our numerical results for $Re = 1.7\times10^5$ show the expected linear behavior of the lift coefficient with the angle of attack, and they are in very good agreement with the Hoerner and Borst (1985) experiments for the laminar flow case ($Re = 1.7\times10^5$). Because the boundary layer is tubulent in the experiments with $\mathrm{Re} = 3.0\times10^6$ (Abbot & Von Doehoff, 1959), the lift coefficient is higher than the other two cases. In adition, our numerical results show a significant improvement over the numerical results obtained also with a vortex method by Akbari and Price (2003), for $Re = 10^4$.

Although not shown, our results for the drag and pressure coefficients on the airfoil indicate the correct physical behavior, but the agreement with experimental results are still approximate, indicating that a better discretization of the vorticity field and smaller time-steps are required to improve the results of the model. Further studies are also being carried out to simulate the stall and post-stalled regimes.

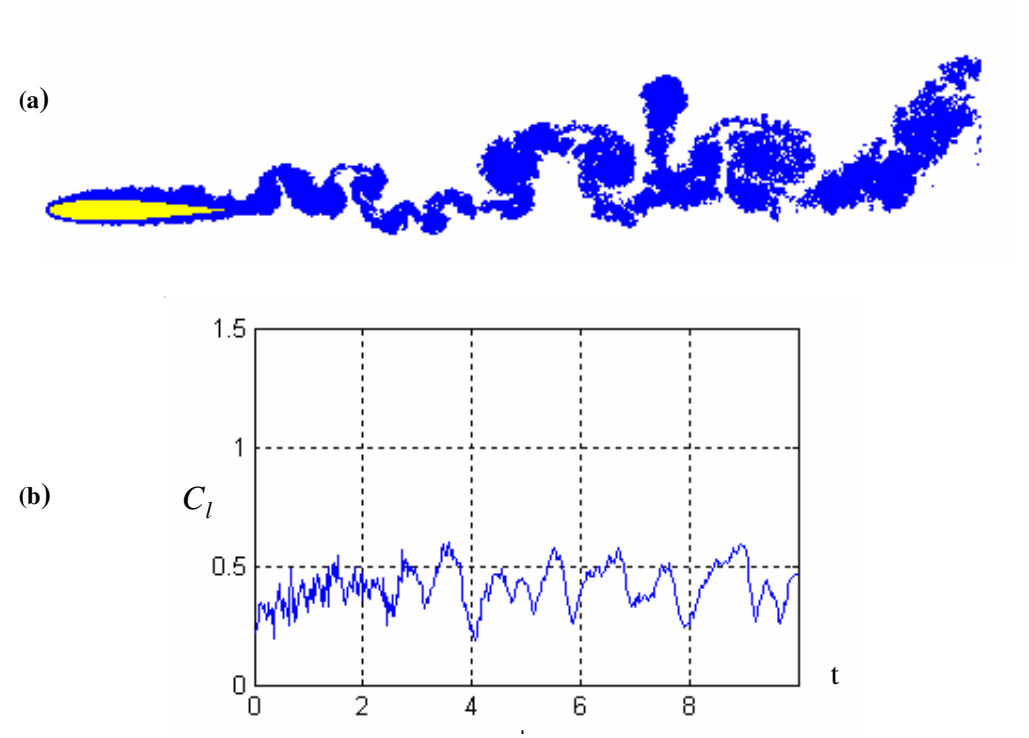

Figure 4. Simulation for $\alpha = 6°$;
(a) Positions of the vortices after 400 time steps; (b) Time evolution of the lift coefficient.

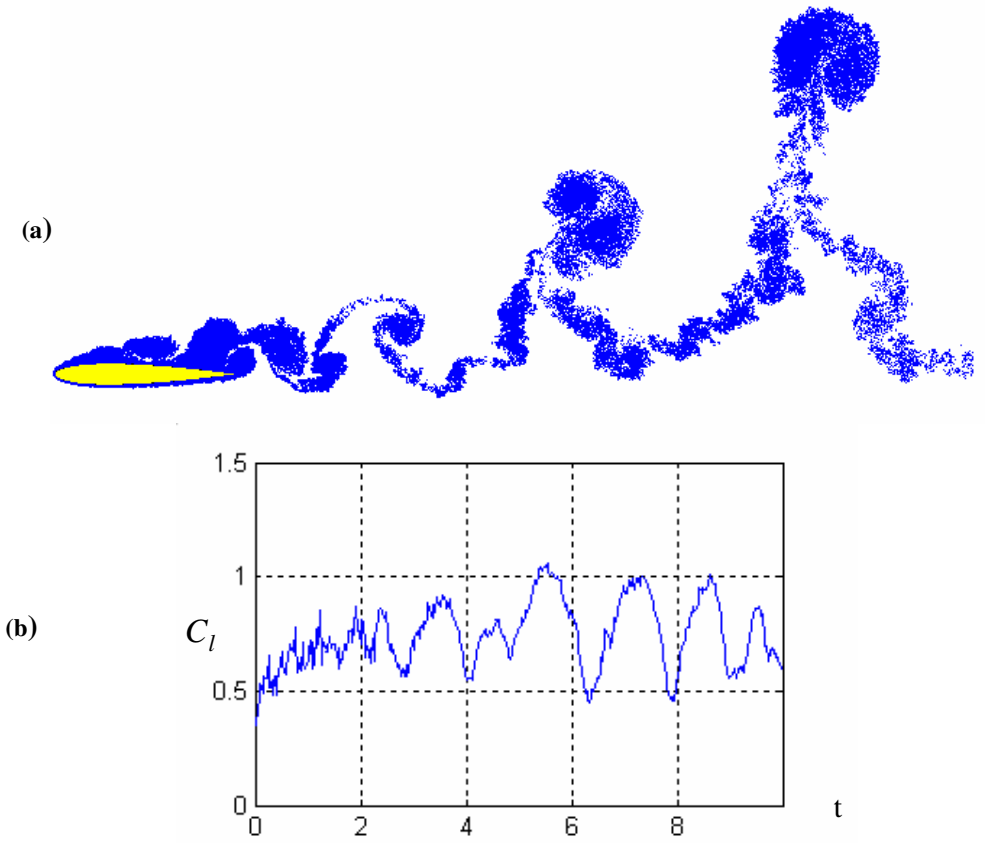

Figure 5. Simulation for $\alpha = 10°$;
(a) Positions of the vortices after 400 time steps; (b) Time evolution of the lift coefficient.

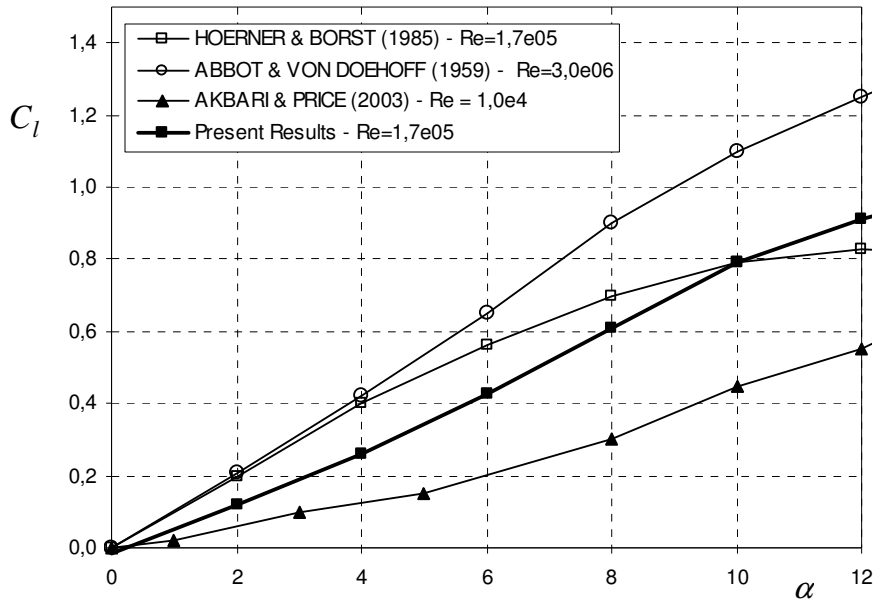

Figure 6. Comparison of the present results with other numerical results and experiments.
Experiments: Abbot & Von Doehoff (1959) and Hoerner & Borst (1985).
Numerical Results: Akbari & Price (2003).

11. Acknowledgements

The authors would like to acknowledge the support from CAPES, through the M.Sc. scholarship of the first author, and CNPq, for the project no. PQ 302246/2004-5 granted to the second author.

12. References

Abbot, I. H., & Von Doehoff, A., 1959, Theory of Wing Sections, Dover Publications, New York.

Akbari, M. H. & Price, S. J., 2003, "Simulation of Dynamic Stall For a NACA 0012 Airfoil Using a Vortex Method", Journal of Fluids and Structures, Vol. 17, pp. 855-874.

Alcântara Pereira, L. A., 1999, "Simulação Numérica do Escoamento em Torno de um Corpo de Forma Arbitrária Utilizando o Método de Vórtice Discretos", Tese de M.Sc., EFEI, Itajubá, MG, Brasil.

Alcântara Pereira, L. A., 2002, "Simulação Numérica do Escoamento ao Redor de Perfis Aerodinâmicos Montados em Grades Lineares de Turbomáquinas Utilizando o Método de Vórtices Discretos com Modelagem Sub-Malha de Turbulência", Tese de D.Sc., EFEI, Itajubá, MG, Brasil.

Chorin, A. J., 1973, Numerical Study of Slightly Viscous Flow, Journal of Fluid Mechanics, Vol. 57, part 4, pp. 785-796.

Guedes, V. G., 2003, "Estudo Numérico do Escoamento ao Redor de Cilindros Circulares e Retangulares Utilizando o Método de Vórtices", Tese de D.Sc., COPPE/UFRJ, Rio de Janeiro, RJ, Brasil.

Hoerner, S. F. & Borst, H. V., 1985, Fluid-Dynamic Lift: Practical Information on Aerodynamic and Hydrodynamic Lift, Hoerner Fluid Dynamics.

Katz, J. & Plotkin, A., 2001, Low - Speed Aerodynamics, 2nd edition, Cambridge University Press.

Lewis, R. I., 1991, Vortex Element Method for Fluid Dynamic Analysis of Engineering Systems, Cambridge, Cambridge University Press.

Martensen, E., 1931, "The Calculation of the Pressure Distribution on a Cascade of thick Airfoils by means of Fredholm Integral Equations of the Second Kind", Aerodynamics Experimental Station, Göttingen.

Mustto, A. A., 2004, "Simulação Numérica do Escoamento Turbulento em Torno de um Cilindro Circular via Método de Vórtices", Tese de D.Sc., COPPE/UFRJ, Rio de Janeiro, RJ, Brasil.

Pereira, L. H. G. & Bodstein, G. C. R., 2004, "Método dos Painéis com Distribuições de Singularidade Quadráticas Aplicados a Escoamentos Bidimensionais sobre Aerofólios", ENCIT – 10 Congresso Brasileiro de Ciências Térmicas, Rio de Janeiro, RJ, Brasil.

Pereira, L. H. G., Silva, D. F. C. & Bodstein, G. C. R., 2004, "Estudo Numérico do Escoamento Potencial em Torno de um Aerofólio Utilizando o Método dos Painéis", ENCIT – 10 Congresso Brasileiro de Ciências Térmicas, Rio de Janeiro, RJ, Brasil.

Sarpkaya T., 1994, "Vortex Element Method for Flow Simulation", Advances in Applied Mechanics, Vol. 31, pp. 113-247.